*Journal of Computational Design and Engineering*, 2021, 8(5), 1191–1203

https://doi.org/10.1093/jcde/qwab040
Journal homepage: www.jcde.org

Downloaded from https://academic.oup.com/jcde/article/8/5/1191/6347742 by National Science & Technology Library Root Admin user on 27 August 2021

RESEARCH ARTICLE

# Generative design and fabrication of a locust-inspired gliding wing prototype for micro aerial robots

Hamid Isakhani [1,*], Nicola Bellotto [1], Qinbing Fu [1,2] and Shigang Yue [1,2]

[1]School of Computer Science, University of Lincoln, Lincoln LN6 7TS, Lincolnshire, UK and [2]Machine Life and Intelligence Research Centre, Guangzhou University, Guangzhou 510006, Guangdong, China

*Corresponding author. E-mail: hamid.isakhani@gmail.com http://orcid.org/0000-0002-7443-371X

## Abstract

Gliding is generally one of the most efficient modes of flight in natural fliers that can be further emphasized in the aircraft industry to reduce emissions and facilitate endured flights. Natural wings being fundamentally responsible for this phenomenon are developed over millions of years of evolution. Artificial wings, on the other hand, are limited to the human-proposed conceptual design phase often leading to sub-optimal results. However, the novel Generative Design (GD) method claims to produce mechanically improved solutions based on robust and rigorous models of design conditions and performance criteria. This study investigates the potential applications of this Computer-Associated Design (CAsD) technology to generate novel micro aerial vehicle wing concepts that are structurally more stable and efficient. Multiple performance-driven solutions (wings) with high-level goals are generated by an infinite scale cloud computing solution executing a machine learning-based GD algorithm. Ultimately, the highest performing CAsD concepts are numerically analysed, fabricated, and mechanically tested according to our previous study, and the results are compared to the literature for qualitative as well as quantitative analysis and validations. It was concluded that the GD-based tandem wings' (forewing and hindwing) ability to withstand fracture failure without compromising structural rigidity was optimized by 78% compared to its peer models. However, the weight was slightly increased by 11% with 14% drop in stiffness when compared to our models from previous study.

*Keywords:* computer-associated design; bioinspired corrugated wings; vacuum thermoforming; additive manufacturing; flexural stiffness; maximum deformation rate

## 1 Introduction

Earliest pieces of evidence on flapping wing aircraft design were probably Leonardo da Vinci's hand drawings of an ornithopter in 1485, followed by Rayleigh's (Rayleigh, 1883) satisfactory report on soaring flight of birds. However, first quantitative analysis of birds' flapping flight was introduced by Walker (1925), which was later elaborately demonstrated in Ellington's contributions on the aerodynamics of hovering insect flight (Ellington, 1984a, b, c). Generally, wings are considered responsible in determining the required thrust to remain airborne. Hence, higher wing efficiencies reduce carbon footprint and propulsion noise while facilitating long-range flights among other advantages. Ultra-high performance wings are possible to find in nature, particularly on certain insects (e.g. dragonflies and locusts) with a tandem wing configuration (Lorenz, 2009; Du & Sun, 2012; Henningsson *et al.*, 2014; Kim & Han, 2014; Hou *et al.*, 2015).

Theoretical, computational, and experimental studies are continuously conducted on such insect wings to better understand the underlying physiological phenomenon responsible for their quality performance (Baker & Cooter, 1979; Kesel, 2000; Kim *et al.*, 2009; Meng & Sun, 2011; Koehler *et al.*, 2012; Xiang *et al.*,

**Received:** 28 February 2021; **Revised:** 14 June 2021; **Accepted:** 15 June 2021

© The Author(s) 2021. Published by Oxford University Press on behalf of the Society for Computational Design and Engineering. This is an Open Access article distributed under the terms of the Creative Commons Attribution-NonCommercial License (http://creativecommons.org/licenses/by-nc/4.0/), which permits non-commercial re-use, distribution, and reproduction in any medium, provided the original work is properly cited. For commercial re-use, please contact journals.permissions@oup.com

2016). These desirable traits mainly include wing morphology offering agile manoeuvres, and Reynolds number-independent flight performance (Levy & Seifert, 2009; Rival *et al.*, 2011; Broering & Lian, 2012; Broering *et al.*, 2012; Henningsson *et al.*, 2015; Luca *et al.*, 2017). Morphological wing geometry is a pivotal factor contributing to the gliding capabilities of these insects (Isakhani *et al.*, 2020a, 2021b). However, even precise geometric characteristics including contour, thickness, corrugations (Luo & Sun, 2005; Tanaka *et al.*, 2015; Chen & Skote, 2016), and even superior mechanical properties considered in the design process may not help evolve beyond a primitive base design concept that is iterated manually using computer-aided design (CAD) software packages.

Although an integrated process flow involving CAD and performance analysis coupled with rapid prototyping has provided an opportunity for designers to move beyond production of final drawings (Jansson & Smith, 1991; Youmans & Arciszewski, 2014; Sharma & Gurumoorthy, 2020; Nguyen *et al.*, 2021), technology has developed far past these limitations with the cloud computing engines capable of infinite scale processing computation-intensive machine learning algorithms that in turn generate thousands of mechanically improved solutions in response to rigorous and robust models of design constraints and performance (Shea *et al.*, 2005; Chakrabarti *et al.*, 2011; Nourbakhsh *et al.*, 2016; Rubaiat *et al.*, 2017). Considering the computer as a collaborative partner in the design process otherwise known as Computer-Associated Design (CAsD) is the next generation of CAD technology. Unfortunately, similar to any nascent form of technological solution, CAsD or Generative Design (GD) presents numerous deficiencies that can be effectively remedied by experimental investigations and extra supervision. Various industries have already implemented this technique in producing novel and feasible designs such as cooling fins and wheel rims (Hoisl & Shea, 2011), gear boxes (Lin *et al.*, 2009), power trains (Helms & Shea, 2012), satellites (Haefer & Rudolph, 2005), and aircraft configurations (Autodesk, 2018).

Similarly, this study explores the application of GD in micro wing design by conducting preliminary evaluation of the solution dataset obtained. In this regard, we conduct a numerical finite element analysis (FEA) on the digitized wings to establish their mechanical performance, stability, and manufacturing worthiness. Ultimately, the approved designs that pass the simulation tests are moved forward to the fabrication process to evolve from a concept to prototypes ready for mechanical testing. Micro wing manufacturing is a precision science that requires utmost subtlety and as such, certain available techniques that disregard a natural wing's accurate corrugations and contours in the process are eliminated from our list of candidate methods (Park *et al.*, 2007; Nguyen *et al.*, 2011; Perez-Rosado *et al.*, 2015). Operation costs and availability, on the other hand, are also crucial constraints that are considered for a more efficient and rapid concept evaluation. As such, several advanced methodologies such as MEMS etching (Pornsin-sirirak *et al.*, 2001; Bao *et al.*, 2011; Bao & Cattan, 2011) and cast micromoulding (Tanaka *et al.*, 2007; Tanaka & Wood, 2010) are also overlooked in this work.

Therefore, to satisfy all the above-mentioned conditions, we introduced a hybridized manufacturing procedure in Isakhani *et al.* (2020b, 2021a), involving three major stages where the digitized insect wing models are three-dimensional (3D) printed (Richter & Lipson, 2011; Lin *et al.*, 2014; Salami *et al.*, 2016; Ceruti *et al.*, 2019; Kim & Yoo, 2020; Takeda *et al.*, 2020; Zhang & Moon, 2021) to act as moulds, which are then processed and placed in a vacuum thermoforming oven (Macdonald, 2006; Engelmann, 2012) to produce affordable polyvinyl chloride (PVC)-based wing prototypes. Finally, $CO_2$-based laser trimming is used to cut through planform and venations precisely. This procedure facilitated the development of wing prototypes with maximum aesthetic and mechanical similarity in comparison to their counterparts in nature.

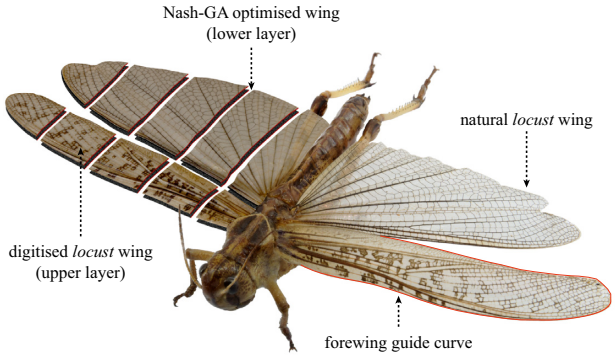


**Figure 1:** Illustration of a typical desert locust with digitized wing sectioned at 20%, 40%, 60%, and 80% spanwise chord, superimposed over its Nash-GA optimized counterpart from Isakhani *et al.* (2020a, 2021b). Profiles highlighted in red are the actual side-view macroscopic images of the sectioned locust wings.

To conclude, an experiment-based mechanical investigation is conducted by subjecting the artificial wing prototypes to a flexural stiffness test (Shang *et al.*, 2009; Jin *et al.*, 2010) and a maximum deformation rate measurement (Liu *et al.*, 2017) in the direction of chord and wingspan to (a) evaluate the application and effectiveness of CAsD technology in aerospace design and (b) highlight the influence of corrugations and membrane reinforcement in the wing development process. Finally, a comparative study reveals the structural performance of wings developed in nature, CAD, and CAsD to provide an insight into the prospects and advantages of each design technology for the future studies.

## 2 Wing Model

This study focuses on the prototyping of a locust's tandem wings. Therefore, we selected and procured several healthy (undamaged wing) farm bred adult female specimens (*Schistocerca gregaria*) shown in Fig. 1 from an insect farm in Cangzhou, China. The locusts were primed for digital pseudo-microscopic scanning by anaesthetizing them with $CO_2$ gas and placing a droplet of high-viscosity cyanoacrylate (superglue) on their wing roots to form gliding posture as described in Taylor and Thomas (2003) and Isakhani *et al.* (2021b). Tandem wings (forewing and hindwing) with a variable thickness ranging from 2 to 3 μm due to venations were both sectioned at 20%, 40%, 60%, and 80% spanwise chord to expose their corrugation profiles necessary for the 3D reconstruction process.

### 2.1 3D digital reconstruction

Initially, the sectioned wings were placed in a light box equipped with an AmScope 45x stereo microscope on a Sony Alpha A6000 SLR camera capable of recording even the most subtle corrugations in the wing profile geometries otherwise known as aerofoils. Being the foundation of this study, the recorded profiles had to be validated against the literature. As such, Walker *et al.* (2009) observation of locust aerofoil coordinates recorded in a smoke flow visualization experiment on the flying locust wing was found to be most (>90%) similar to our recorded aerofoil

Downloaded from https://academic.oup.com/jcde/article/8/5/1191/6347742 by National Science & Technology Library Root Admin user on 27 August 2021

coordinates in the 2D space digitized from the sectioned wing profiles. Therefore, the coordinates were passed on to the next stage for digital reconstruction in SolidWorks. It must be noted that the insect body effects are assumed negligible as this study focuses on the structural performance of the wings in gliding flight. Furthermore, 2D CAD profiles were converted into 3D wings using the image recordings of locust wings in all three directions (front, top, and side) involving significant information on the planform, forewing and hindwing transverse and longitudinal spacing. Collection of these data facilitated sweeping of a thin solid boss section through the 2D profiles (wing cross-sections at 20%, 40%, 60%, and 80% spanwise chord) along the guide curves defined by contour of the wing planform shown in Fig. 1.

## 2.2 Nash-GA optimized wings

In order to compensate for the precision limitations in the digital reconstruction process, wing profiles (aerofoils) are subjected to an aerodynamic optimization methodology introduced in the first stage of our work (Isakhani *et al.*, 2021b). This paper, on the other hand, introduces a mechanical optimization process and since the aerodynamic and structural performances of a wing are strongly correlated, a brief description of the previous aerodynamic optimization process is provided to better comprehend the influence and correlation of these two properties. Digitized wing profiles are treated as conventional aerofoils that are systematically parametrized with the help of the PARSEC method and optimized using a novel fusion of Nash strategy and genetic algorithms (GAs).

A non-cooperative multiple objective optimization technique introduced by Nash (1951) is fused with the bioinspired GAs that is based on an adaptive heuristic search approach inspired by the natural selection and genetics (Haupt & Haupt, 1998). A combination of the two schemes produces a two-player Nash equilibrium game strategy (D'Amato *et al.*, 2012a, b) with the coefficients of lift and drag being the two players. Parametrization, being the foundation of a geometrical optimization process, is responsible for transforming a physical problem into a mathematical one by encoding a geometrical shape to form a number of variables. Here, we adapt and implement a reliable aerofoil-specific parametrization scheme developed by Sobieczky (1998), which is based on the idea of expressing an aerofoil geometry as a linear combination of unknown base functions with 11 major attributes assigned to the well-established aerofoil shape parameters. These parameters are selected as the aerofoil's control variables such that the ultimate shape shall be determined by solving a linear system.

For the optimization part, a Nash-improvised GA is implemented that optimizes multiple objective/cost functions non-cooperatively. This facilitates a simultaneous maximization/minimization of two separate objective or cost functions called players (lift and drag). In our case particularly, player-1 (lift) is the objective function and player-2 (drag) is the cost function that must be maximized and minimized, respectively. Furthermore, these players are assigned with different physical design variables (DVs) with a varying dependence level. These DVs are the aerofoil geometric characteristics such as leading-edge angle of incidence, leading-edge radius ($r_e$), profile thickness, etc. parametrized as a result of the PARSEC method. Detailed explanation and dependence levels of these DVs on each player are given in Isakhani *et al.* (2021b). After the implementation of the optimization, in order to evaluate the obtained Nash equilibrium ($N$) with different strategies, we consider all combinations possible for a PARSEC parametrization. The proposed optimization process is performed on all the locust tandem wing cross-section profiles to form the whole-optimized wing shown in Fig. 1. The process is performed at 75% of the original PARSEC parameters (i.e. 25% reduction in each parameter defining aerofoil geometry), with no geometric and aerodynamic constraints. Reduction in the parameters is justified by the fact that PARSEC variable contraction results in further streamlining of an aerofoil. Also, the value 25% is selected specifically in accordance with the related literature (Della Vecchia *et al.*, 2014) to devise a fair comparative study. Please refer to Isakhani *et al.* (2021b) for detailed method description and performance validations.

## 2.3 CAsD

The involvement of computer in the designing of a digital model is known as CAsD. This technology is a hybridization of design and optimization process integrated usually in a computation-intensive machine learning algorithm executed on a powerful cloud computing technology. In this study, the GD in Autodesk® Fusion 360 running on Autodesk® Cloud Services with an unlimited Education License is hired to experiment with the novel design solutions that can be generated in response to our rigorous and robust models of design constraints and performance. As seen in Fig. 3, the process flow for CAsD comprises a closed-loop feedback system that accepts design conditions, starting geometry, and the target performance as an input explained in the following sections.

### 2.3.1 *Design space*

Initially, design space is defined for the algorithm. In this study, we present two different configurations of design spaces. Initially, the 'unguided' case shown in Fig. 2a takes input geometry (preserved) as a 0.05-mm-thick solid frame representing a locust forewing planform. A rectangular solid (obstacle geometry) shelled in the shape of the wing corrugations provides an empty space (maroon) similar to a canvas for the algorithm to create venation pattern that maintains precise corrugations. On the other hand, the 'guided' case shown in Fig. 2b takes the locust venation pattern into consideration while generating the design outcome. That is, the preserved geometry remains the same; however, the obstacle geometry is designed as a mould of the natural locust wing with venations in contrast to the previous case where the obstacle geometry was only a mould of the locust wing surface without venations. In this case, the association of computer in the design process is relatively limited since the guiding pattern (obstacle geometry) dictates the ultimate design outcome to a great extent.

### 2.3.2 *Design conditions*

As the next stage of the problem definition, loads and constraints are determined for the algorithm. Shown in Fig. 5, a distributed load (blue arrows) is applied uniformly on the preserved geometry to represent the amount of upward force (acting as the point force in a flexural stiffness test) that the design is expected to bear with minor elastic deformation. Gravity (yellow arrow) acts in the opposite direction of the applied force, and the fixed constraint face (lock) shown in red colour is placed at the wing root to limit the degree of freedom (DOF) spanwise.

### 2.3.3 *Designs exploration*

The machine learning algorithm processes the data and generates thousands of mechanically improved design solutions that are quantitatively and qualitatively evaluated in terms of

Downloaded from https://academic.oup.com/jcde/article/8/5/1191/6347742 by National Science & Technology Library Root Admin user on 27 August 2021

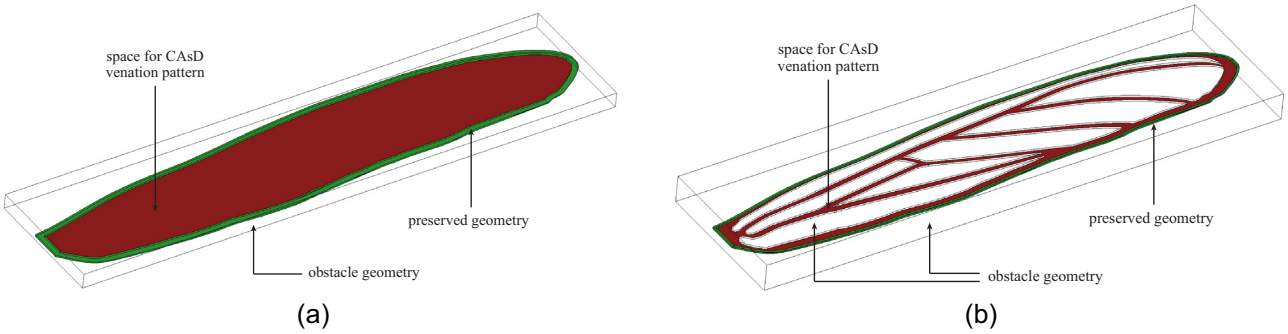


**Figure 2:** Illustration of the two design space configurations defined for the CAsD algorithm in this study; (a) unguided space without venations, and (b) guided space with venation pattern.

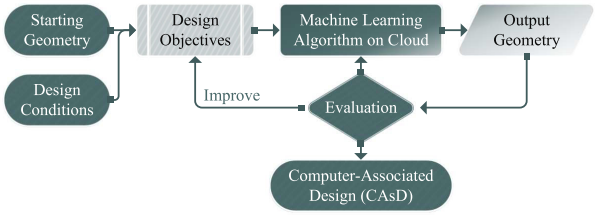


**Figure 3:** Illustration of the process flowchart to achieve a functional CAsD model.

various mechanical properties such as mass, density, factor of safety, maximum von Mises stress, flexural stiffness, and even aesthetics. Aesthetic properties are important to ensure a visually similar structure when compared to an actual wing's venations that is responsible to reinforce and shape the delicate wing membrane according to the corrugations. This is because the algorithm often generates certain unconventional designs that do deliver the required mechanical performance but fail to satisfy several other functions such as a relatively uniform distribution of venations.

Next, the obtained results are fed back into the loop as an individual iteration to enhance the designs in future cycles until the ultimate desirable solution called the final CAsD model is achieved. The stopping criteria defining the desirability of the ultimate solution are a set of design objectives such as weight optimization and required factor of safety designated prior to execution of the CAsD generative algorithm. Several design solutions converged after tens of iterations deliver the optimum performance defined in the design objectives. Shown in Fig. 6 are some of the converged wing designs for two different materials, namely PVC (triangles) and Aluminium (circles) indicated in blue and red representing forewing and hindwing designs, respectively. Although we aim to fabricate our wing prototypes only in PVC, we have included the aluminium-based designs for the sake of expanding the scope of our solution exploration.

As mentioned earlier, aesthetics and visual properties play an important role in the final design selection. However, a well-balanced design trade-off strategy must be established to take mechanical properties into consideration as well. Therefore, the PVC-based designs with >5.0 factor of safety capable of bearing >2 MPa of maximum von Mises stress successfully pass the visual inspection and are recommended for further advanced FEA. Figure 4a shows the two recommended CAsD models of forewing and hindwing that are generated purely based on performance requirements and design space shown in Fig. 2a. The so-called performance is referred to the structural stability that the wing designs must deliver upon application of the loads and constraints numerically defined for the CAsD algorithm. Design constraints and objectives are defined equally for all the models to evaluate the performance of the CAsD algorithm accurately. Main built-in objective functions such as factor of safety and mass optimization intensity are set as 2.0 and 100%, respectively. The percentage implies our maximum targeted weight reduction. Therefore, 100% means that the ultimate design solutions must be optimized to their fullest potential.

The wing model shown in Fig. 4b, on the other hand, is the outcome of the design space shown in Fig. 2b where the locust-inspired venation pattern is taken into consideration. In this case, the association of computer in the design process is relatively limited since the obstacle geometry dictates the ultimate design outcome to a great extent, such that the converged design seen in Fig. 4b is no more considered for fabrication due to its excess similarity with our previous locust-inspired artificial wing design (VT-1c) that is already available for the comparative study in the following sections, and also its failure to satisfy the minimum material requirement for the manufacturing purposes. It can be noted that the initially unguided CAsD wing shown in Fig. 4a is bulkier with material concentration at certain regions; this is mainly due to the limitations of the novel CAsD technology that considers only mechanical properties ignoring remaining parameters such as aerodynamic performance, therefore generating only locally optimized designs. Furthermore, in an attempt to address all the aforementioned limitations, aesthetic inspections are conducted to select the most suitable designs for further numerical analysis. The term 'suitable' used here is a comparative adjective that does not necessarily imply that the selected model is optimized or aesthetically best design solution, but it is only a reference to the aesthetically best solution amongst all the available CAsD generated designs.

## 3 FEA

The 3D CAsD generated models of the locust tandem wings shown in Fig. 4a were initially subjected to a comprehensive numerical analysis of its mechanical performance in ANSYS® Workbench to establish its manufacturing worthiness prior to the fabrication process (Yang *et al.*, 2021). Due to the limitations in the processes involved in fabrication such as laser cutting, it is necessary to adapt the CAsD models such that inaccurate and overlapping piercings are avoided by the laser beam. This may be caused due to excessively narrow venation patterns generated by CAsD. Therefore, we edit and adapt the

Downloaded from https://academic.oup.com/jcde/article/8/5/1191/6347742 by National Science & Technology Library Root Admin user on 27 August 2021

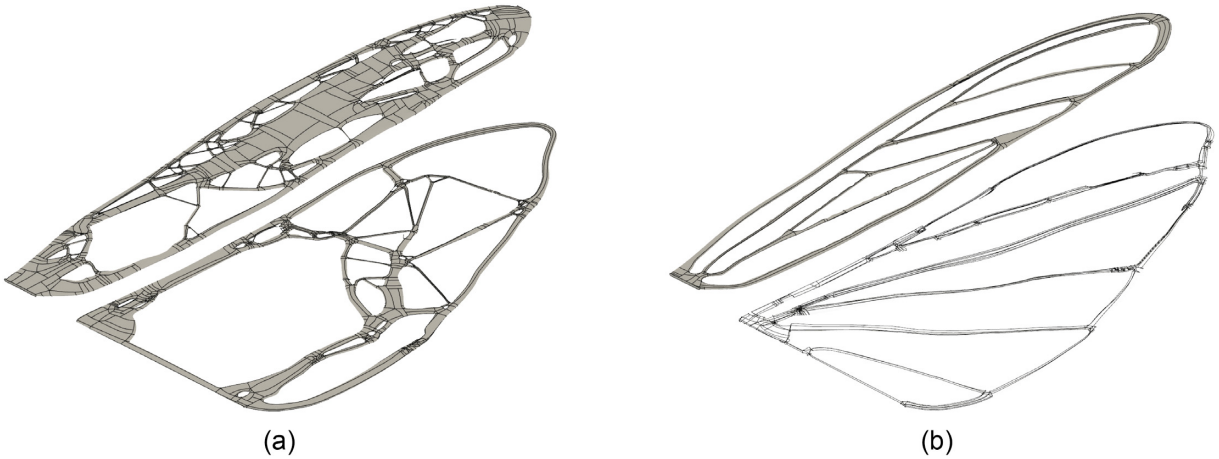


**Figure 4:** CAsD converged tandem wings; (a) with unguided and free-form GD space incorporating no venations, and (b) with locust-inspired GD space consisting of venation patterns.

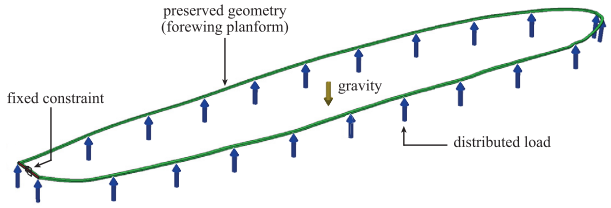


**Figure 5:** Illustration of the design conditions including distributed load and fixed constraint application on the preserved geometry spanwise.

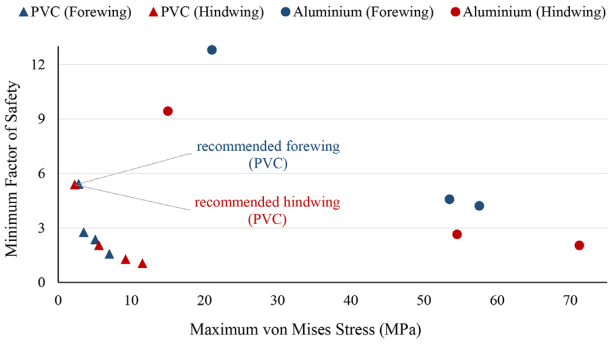


**Figure 6:** Graphical representation of the converged wing designs for two different materials, namely PVC (triangles) and Aluminium (circles) coloured in blue and red corresponding to forewing and hindwing designs, respectively.

models slightly and compare their performance numerically in this section.

Primarily, the digital models are meshed carefully as it is crucial to generate as much structured grids as possible to increase the solution accuracy and computation performance of the analysis. In this case, the heavily refined meshed body consisting of 400 thousand elements produced satisfactory solution with no significant change (< 5%) in the computed deformations upon further refinement. Later, boundary conditions were defined by constraining the wing roots and leading edge to a single rotational DOF about the *X*- and *Y*-axes for the estimation of flexural stiffness chordwise and spanwise, respectively. Since the axilla that is responsible for 3D motion of the wings was not considered in our model, we ignore the other two DOFs. Finally, a point force (structural load) equivalent to the aerodynamic forces acting on the real locust wing was uniformly applied at almost 70% of the wingspan and chord for the estimation of flexural stiffness spanwise and chordwise, respectively.

The static structural solution of the CAsD models involved a set of quantitative and qualitative results demonstrating the directional and total deformation, and equivalent (von-Mises) stress/strain distribution. As an example, Fig. 7 shows the equivalent (von-Mises) stress distribution over the simulated wing prototypes: unedited VT-1gd(FEA) and the VT-1gd(FEA). It is evident that the stress concentration at the wing roots has increased and expanded towards the wing tip as a result of the load application on the original CAsD design seen in Fig. 7a. However, upon adaptation of the model VT-1gd shown in Fig. 7b, stress concentration towards the wing roots for both the forewing and hindwing is simultaneously reduced. Although the maximum stress experienced by the unedited VT-1gd(FEA) is yet to exceed midway through the safety factor, the process of editing and adaptation further increases the factor of safety. A clear relationship between the experimental and numerical results is established and determined such that their differences are found to be negligible, further bolstering the reliability of the experimental set-up and the results obtained. Having established manufacturing worthiness, the models are carried forward to the fabrication stage.

## 4 Fabrication Methods

Detailed study of different feasible fabrication processes is provided in our previous papers (Isakhani *et al.*, 2020b, 2021a). Here, we employ the most efficient combination of manufacturing techniques involving fused deposition modelling (FDM) 3D printing, vacuum thermoforming, and laser Computer Numerical Control (CNC) machining process. Initially, the 3D CAD geometries are additively manufactured with the utmost precision to maintain the actual corrugations scanned from the locust natural wings. The 3D printed wings with 100% base infill act as moulds for the casting process that involves a fully automated vacuum thermoforming machine moulding PVC sheets of varying thicknesses into an extremely lightweight, resilient, and affordable wing prototype. Finally, post-processing involves $CO_2$ laser cutting that is necessary for a precise trimming of the wings along their planform and venation patterns removing the

Downloaded from https://academic.oup.com/jcde/article/8/5/1191/6347742 by National Science & Technology Library Root Admin user on 27 August 2021

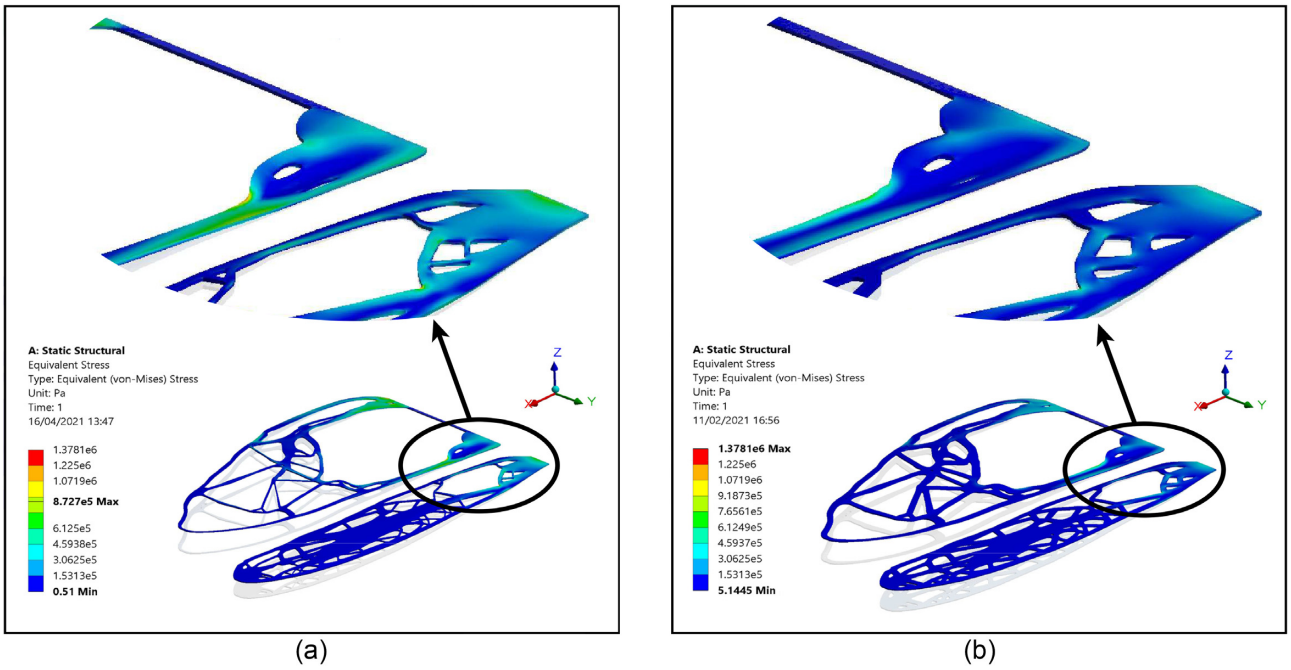


**Figure 7:** Illustration of the equivalent (von-Mises) stress distribution contour over the CAsD-developed locust-inspired tandem wings; (a) unedited VT-1gd(FEA) and (b) VT-1gd(FEA).

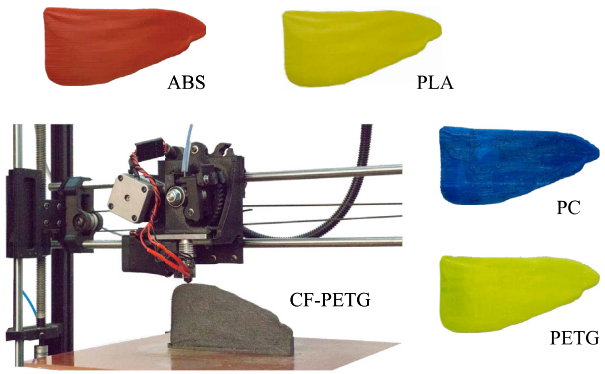


**Figure 8:** Additive manufacturing (FDM) of the wing moulds using a variety of commonly available materials, namely PLA, ABS, PETG, PC, and carbon fibre infused PETG (CF-PETG).

peripheral membrane that shall be replaced by 15-μm PVC wrap further optimizing weight and flexibility.

## 4.1 Additive manufacturing

Since the number of sample prototypes required to be produced is limited for experimental purposes, the preparation of an aluminium mould that is more appropriate for vacuum thermoforming is not taken into consideration. Therefore, a readily available and economical manufacturing method such as desktop 3D printing (FDM) is hired to fulfil the task of our mould preparation. In particular, we use a consumer-grade intermediate-user 3D printer (Taz5 LulzBot®, Aleph Objects, Inc. Colorado, United States) operating on the Cura LulzBot Edition 3.6.18 slicing software shown in Fig. 8. To account for the wing corrugations being precisely reflected by the moulds, their printed cross-section must remain reasonably thin (≤1 mm). To achieve this, we modify the extruder nozzle's material and diameter from 0.5-mm brass to 0.25-mm stainless steel facilitating higher precision in the mould preparation process. However, since the casting involves elevated temperatures, robustness and thermal resistance of the moulds must not be compromised as a result of overrefinement.

Additionally, 3D printer-induced challenges such as warping and overhang problems further restrict our choice of printing filament as well. Hence, a balanced trade-off strategy must be established to determine the most appropriate printing thickness and material addressing our objectives collectively. Although manufacturing and testing of both locust-inspired forewing and hindwings are performed in this study, hindwing moulds are presented in this section for illustration of its geometrical features since the following sections mainly focus on the illustration of the forewings. To explore different combinations of settings and configurations, we experimented with a variety of commonly available printing materials shown in Fig. 8 including Acrylonitrile Butadiene Styrene (ABS), Polylactic Acid (PLA), Polycarbonate (PC), and Polyethylene Terephthalate Glycol (PETG). Detailed mechanical properties for different filament materials are provided in Table 1 (some data from Simplify3D®). It can be observed that the quantitative properties associated with the materials tabulated are strongly in agreement with the qualitative data being the visual appearance of the moulds in Fig. 8. For instance, the polycarbonate hindwing mould has the poorest print quality although its strength and durability are highly favourable.

Similarly, each filament has certain properties that are advantageous and must be fused to obtain a single material with maximum desirable traits. As seen in Table 1, the flexibility and printability of PETG are attractive properties; however, specific strength and thermal stability of carbon fibre are required for the heated casting (thermoforming) process. Thus, a fusion of

Downloaded from https://academic.oup.com/jcde/article/8/5/1191/6347742 by National Science & Technology Library Root Admin user on 27 August 2021

**Table 1:** Material properties of different 3D printed wing moulds.

| Mould printed material | Maximum resolution (μm) | Minimum profile thickness (μm) | Mould density (g/cm$^3$) | Stiffness rate (%) | Coefficient of thermal expansion (μm/m°C) | Ultimate strength (MPa) | Durability rate (%) | Printability rate (%) |
|---|---|---|---|---|---|---|---|---|
| PLA | 140 | 250 | 1.24 | 75 | 68 | 65 | 40 | 90 |
| ABS | 150 | 250 | 1.04 | 50 | 90 | 40 | 80 | 80 |
| PC | 250 | 500 | 1.2 | 60 | 69 | 72 | 100 | 60 |
| PETG | 150 | 250 | 1.23 | 50 | 60 | 53 | 80 | 90 |
| CF-PETG | 180 | 250 | 1.3 | 100 | 57.5 | 68 | 30 | 80 |

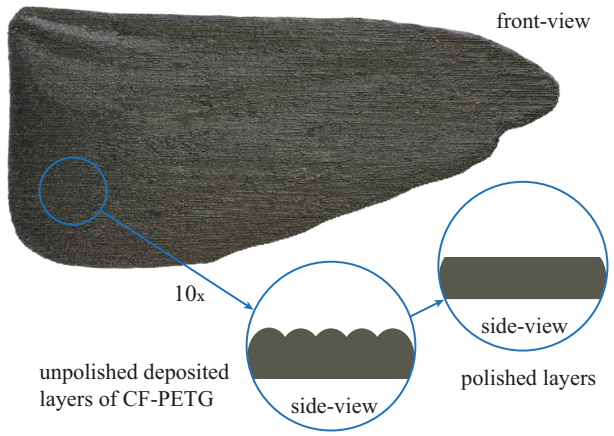


**Figure 9:** Post-processing (polishing) of the wing moulds using sandpapers with grits from 500 to 2000 incremented in 250 grits to achieve precise removal of only the micro humps resulted from additive layer deposition.

these two materials (CF-PETG) shown on the printer bed in Fig. 8 is found to satisfy our strict requirements by delivering a high (100%) stiffness and printability rate and a low (57.5 μm/m°C) coefficient of thermal expansion. Ultimately, the post-processing involved polishing and treating the mould surfaces with a set of sandpapers with grits from 500 to 2000 incremented in 250 grits to compensate for the minor roughness developed as a result of layered material deposition involved in FDM additive manufacturing. As seen in Fig. 9, this step facilitates the removal of micro humps resulted from the FDM-based 3D printing. The delicate removal of the humps ensures smooth and precise curing of corrugations onto the final prototypes.

## 4.2 Vacuum thermoforming

For the moulding process, we hired a fully automatic vacuum thermoforming machine shown in Fig. 10, which satisfies our strict prerequisites being cost effectiveness, ease of operation, and accessibility of the raw materials and machinery involved in the fabrication process. This industrial manufacturing method is widely used in the mass production of packaging and disposable containers. This study explores the potentials and proposes the application of these machines for the future mass production of parts for the lightweight micro class of expendable bioinspired drones. An automated thermoforming machine can produce hundreds of parts in a matter of minutes shown in the supplementary multimedia files. For our limited sample development, we hired a local small-volume production facility along with one technician for two hours producing three hundred individual pieces of wing prototypes.

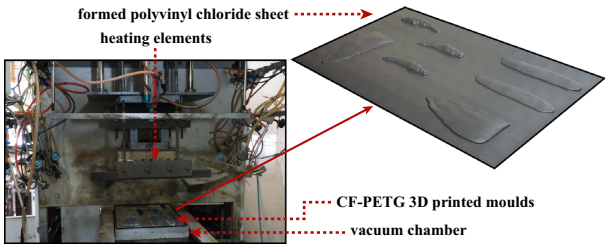


**Figure 10:** Fully automatic vacuum thermoforming chamber rapidly heating and pressing 150-μm-thick PVC sheets onto the 3D printed moulds to form PVC-based locust wing and body prototypes (VTs).

The overall process involves the preparation of the mould basements that must be flattened with a modelling clay and fixed onto the steel tray custom-made to fit the machine's moulding frame as seen on the right of Fig. 10. Later, PVC sheets of different thicknesses (150–250 μm) were fed into the machine similar to a paper printer. The plastic sheets are rolled over the moulding frame that is heated to 130°C (pliable temperature of PVC) and exerted with a negative pressure to form the exact shape of the wing moulds laid on the tray. It must be noted that even the smallest dust particle on the moulds is formed onto the PVC sheets; hence, a clean environment is recommended to maintain precision. Finally, a couple of nozzles spray cooling fluid on the moulded sheets to release the material feed for the next-forming iteration. As mentioned earlier, CNC machined aluminium moulds are more suitable for this manufacturing technique; however, due to our limited production volume and extra precision requirements, we opted for the more economical carbon infused PETG moulds that remained rigid throughout the forming process and functioned better than expected. PVC sheets of various thicknesses were used to develop distinct prototypes (VT-1,2), to better understand the influence of prototype thickness on its mechanical properties, and facilitated an informed identification of the desirable wing prototypes for different applications and requirements.

## 4.3 $CO_2$ laser CNC

To achieve extra precision in the post-processing of the prototyped wings, we employ a $CO_2$-based 10.6-μm wavelength laser CNC machine to trim the thermoformed PVC sheets along the contours of the wing planform and venation patterns for each design individually as shown in Fig. 12. Since our working material (PVC) is highly plasticized at elevated temperatures (>130°C), an individual trial and error for each wing design and PVC thickness must be performed to calibrate the laser power and speed.

Downloaded from https://academic.oup.com/jcde/article/8/5/1191/6347742 by National Science & Technology Library Root Admin user on 27 August 2021

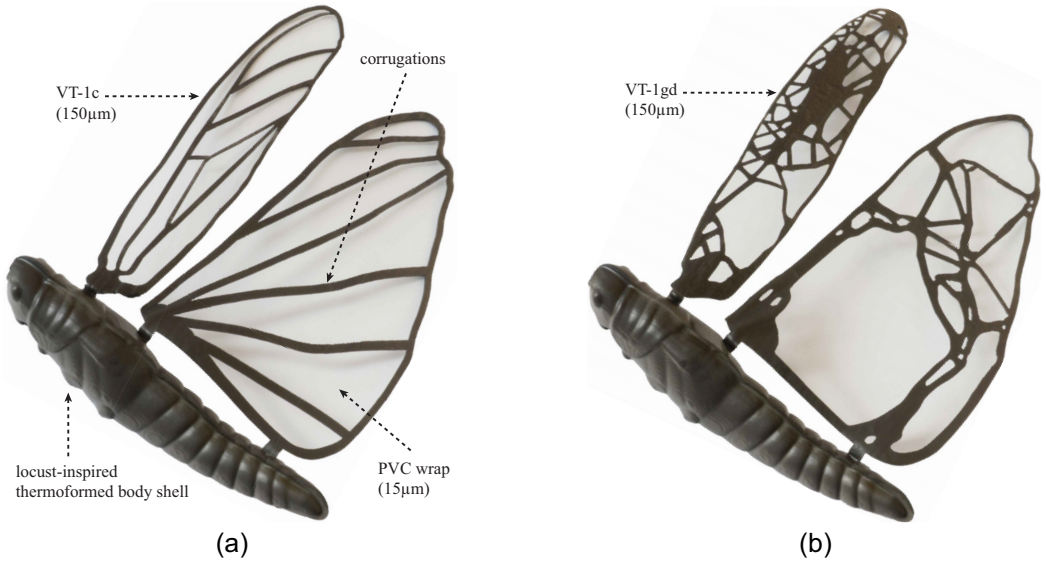


**Figure 11:** Vacuum thermoformed PVC wing prototypes fixed on a VT locust body frame; (a) 150-μm-thick forewing and hindwing (VT-1c) with locust-inspired venations, and (b) 150-μm-thick forewing and hindwing (VT-GD) with CAsD venations.

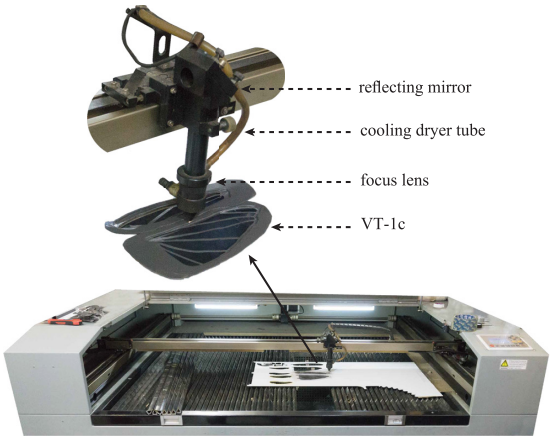


**Figure 12:** $CO_2$ laser CNC cutting machine trimming the locust-inspired thermoformed PVC body, wings, and venation patterns producing CAD and CAsD prototypes (VT-1c and VT-1gd).

As an example, 15 W and 40 $ms^{-1}$ were set for cutting the VT-1c wing that is 150 μm thick, shown in Fig. 11a.

Furthermore, a mirrored forewing and hindwing planform contour is cut out of a medium-density fibreboard (MDF) shown in Fig. 12, which serves as a stencil where the prototype securely locks in place for the laser head to trim accurately through the defined paths. It must be noted that the cutting contours especially for the CAsD prototypes (VT-1gd) shown in Fig. 4a must be adapted for the laser cutting process to achieve the model in Fig. 11b. Due to the sensitivity of PVC sheets particularly at 150 μm thickness, venation contour adaptation is mandatory in addition to a precise laser power calibration to avoid inaccurate and overlapping piercings by the laser beam caused due to excessively narrow venation patterns generated by the computer. Salient advantages of $CO_2$ laser trimming include high pinpoint precision especially for thinner non-metallic materials, cleaner piercing (due to debris absorption), ease of access and operation, low cost, and repeatability.

## 5 Mechanical Testing

Numerous factors influence the mechanical properties of insect wings. One such vital element is the blood (haemolymph) circulated through venations extended over their entire wing surface. This phenomenon was first observed in the grasshopper wings (a member of the *locust* family) by Baker in 1744 (Baker, 1744). Further study on the topic (Hou *et al.*, 2015; Rajabi *et al.*, 2016; Pass, 2018; Tsai *et al.*, 2020) has proved that life (blood circulation) exists in almost all flying and non-flying insect wings. A detailed investigation of its effects on the wing mechanical properties is provided in our previous study (Isakhani *et al.*, 2021a). Among a diverse group of common flying insects, it was proven that the *locust* wing is the most appropriate source of inspiration for artificial wing designs due to their minimum dependence on haemolymph flow-induced flexibility. Similarly, we evaluate the mechanical properties of the artificial wing prototypes developed in this research and summarize in a comparative study to bolster the credibility of our proposed design and manufacturing methods. In particular, we investigate the flexural stiffness and maximum deformation rate in spanwise and chordwise direction of the wings experimentally to demonstrate the influence of material, wingspan-to-thickness ratio, and corrugations on the wing's structural stability. A total of 10 samples are tested that are described in Table 2 as (a) natural *locust* forewing, (b and c) VT-1,2 being uncut 150 and 300 μm, (d) VT-1p that is a laser cut non-corrugated (unformed) 150-μm wing, (e and f) VT-1c,1cs the laser cut 150 μm thermoformed 15 μm PVC wrapped and unwrapped frame wings, and (g–j) VT-1gd, -1gds, -2gd, -2gds being the laser cut GD 150 and 300 μm thermoformed 15 μm wrapped and unwrapped frame wings.

### 5.1 Flexural stiffness

A fundamental wing mechanical property relating the aerodynamic loading and deformation is known as the flexural stiffness. This relationship is measured to validate our prototypes' balanced rigidity and flexibility when compared to the peer models available in the literature. It is categorized as a non-destructive test (NDT) due to its subject reusability, hence

Downloaded from https://academic.oup.com/jcde/article/8/5/1191/6347742 by National Science & Technology Library Root Admin user on 27 August 2021

**Table 2:** Manufacturing processes involved in the fabrication of each prototype.

| Prototype | Description |
|---|---|
| VT-1 | uncut, thermoformed 150 μm PVC |
| VT-2 | uncut, thermoformed 300 μm PVC |
| VT-1p | cut, non-corrugated (not thermof.) 150 μm |
| VT-1c | cut, 150 μm thermof., 15 μm PVC wrapped |
| VT-1cs | cut, 150 μm thermof., 15 μm PVC unwrapped |
| VT-1gd | cut, CAsD, 150 μm thermof., 15 μm wrapped |
| VT-1gds | cut, CAsD, 150 μm thermof., 15 μm unwrapped |
| VT-2gd | cut, CAsD, 300 μm thermof., 15 μm wrapped |
| VT-2gds | cut, CAsD, 300 μm thermof., 15 μm unwrapped |

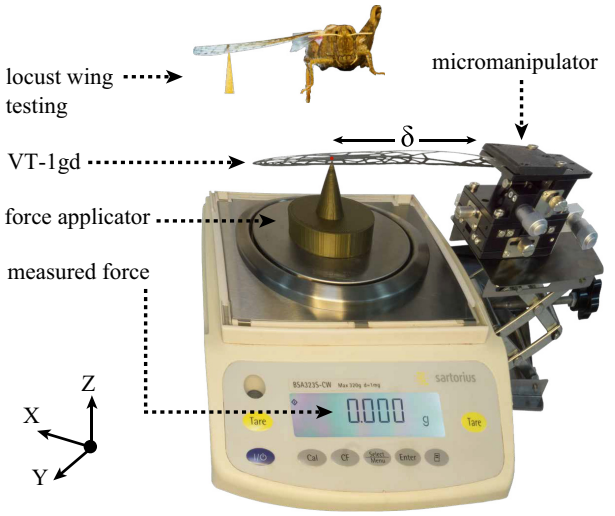


**Figure 13:** Illustration of the flexural stiffness test set-up comprising of an electronic microbalance and a three-axis micromanipulator investigating the VT-1gd forewing prototype along with the real testing of locust forewing.

prioritized with a set-up that is standard according to the literature (Shang *et al.*, 2009; Jin *et al.*, 2010). It consists of an electronic microbalance (Sartorius BSA323S-CW, China), and a three-axis manual micromanipulator (Shengling, LD60-RM, China) fitted with 10-μm-precision micrometre-actuated linear slides. The prototyped wing root is clamped onto the left edge of the micromanipulator platform with its chord parallel to the *XY* plane.

Here, the aerodynamic forces acting on the wing are assumed to be a concentrated point force exerted with a pin fixed vertically on the microbalance at almost 70% of the wingspan and chord for the estimation of flexural stiffness spanwise and chordwise, respectively. Upon counterclockwise rotation of the Z-axis micrometre, the pin comes in contact with the wing placed at a distance ($\delta$) from wing clamp and leading edge for spanwise and chordwise measurement, respectively. Figure 13 shows the exact force points marked on the wing prototypes. The reading on Z-axis micrometre is considered as the wing displacement ($\Delta$). Hence, flexural stiffness (Combes & Daniel, 2003; Shang *et al.*, 2009) can be estimated as $EI = \frac{f\delta^3}{3\Delta}$, where $f$ is the applied static force recorded on the microbalance, with the wing displacement ($\Delta$) limited to 5% of $\delta$, as $EI$ reflects only minor deformation rate.

Figure 14 presents a plot of the flexural stiffness measured for all the wing prototypes developed in this study. It consists

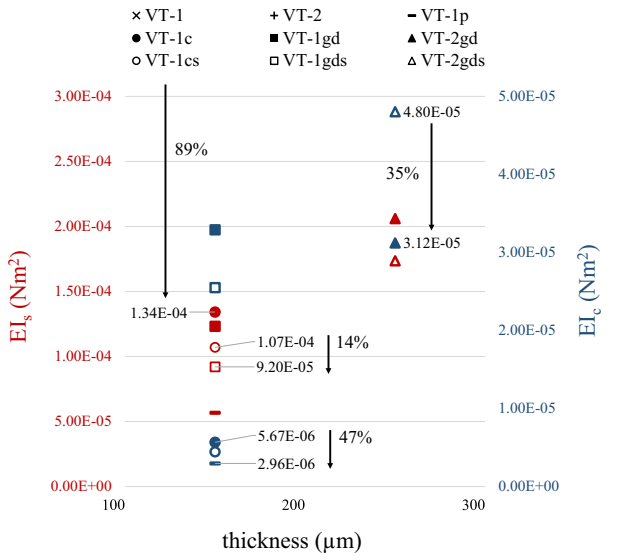


**Figure 14:** Illustration of the flexural stiffness spanwise (red) and chordwise (blue) plotted for different wing prototypes with varying thicknesses.

of nine different plot markers (triangle, square, circle, etc.), each corresponding to a different forewing prototype categorized into two groups of red and blue coloured plots representing the flexural stiffness measured in spanwise ($EI_s$) and chordwise ($EI_c$) direction, respectively. However, the cross and plus marker plots representing VT-1,2 are not presented in the graph since they were out of the nominal range set by the laser-cut wings.

It is a fairly obvious fact that in almost all cases wing thickness is directly proportional to the measured rigidity; i.e. with an increase in PVC thickness, weight and stiffness of the prototype escalate compromising the desired flexibility. Therefore, even the lightest and thinnest (150 μm) wing developed in this study offers twice the stiffness of a natural locust wing. Nevertheless, greater rigidity is necessary to withstand the required wing loading for real-world UAV applications. This is achieved by scaling the prototypes (3x in this case), causing an inevitable increase in wingspan-to-thickness ratio. Additionally, the flexural stiffness measured in spanwise compared to the chordwise $EI$ is found to be greater by an order of a magnitude that is in line with the published literature, further validating the experiments presented in this study. However, the most significant discovery of this analysis highlights the influence of membranes and corrugations on the mechanical properties of the wing prototypes that is elaborated in the Discussion section.

## 5.2 Maximum deformation rate

Another fundamental factor characterizing wing capacity to withstand fracture failure is known as the maximum deformation rate. A test platform similar to the previous set-up is used for the measurement of this property seen in Figs. 15 and 13 where the wing root is again fixed to the edge of the micromanipulator using a clamp. With the help of a pin fixed vertically on an electronic microbalance, the representative aerodynamic forces are applied at 70% of the wingspan and chord for spanwise and chordwise measurement, respectively. The procedure for the measurement of the maximum deformation rate is different from the flexural stiffness evaluation only in terms of the applied wing displacement ($\Delta$) exceeding far beyond 5% until the

Downloaded from https://academic.oup.com/jcde/article/8/5/1191/6347742 by National Science & Technology Library Root Admin user on 27 August 2021

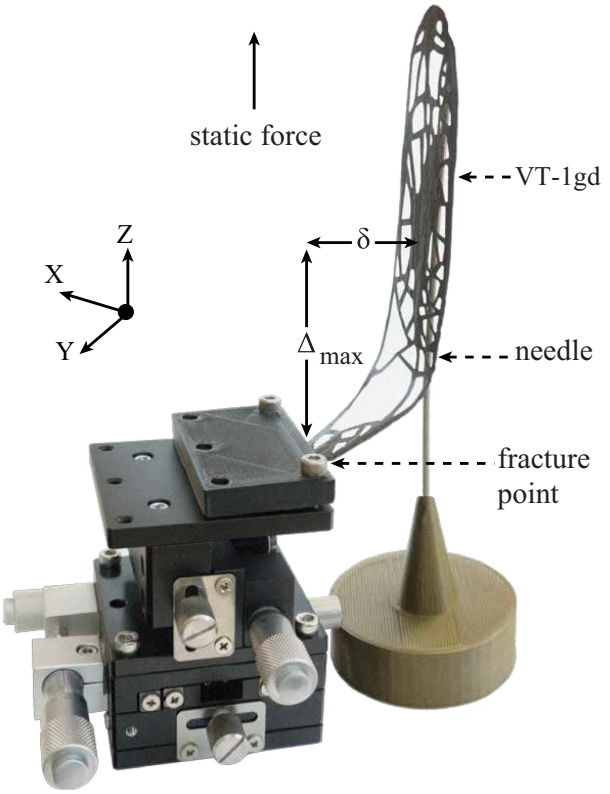


**Figure 15:** Illustration of the maximum deformation rate measurement set-up, VT-1gd undergoing a large deformation (>135.8%) without fracture.

yield strength of the material is surpassed, causing a visually evident plastic deformation (fracture failure). However, in contrast to the brittle carbon fibre and 3D printed wings introduced in the literature (Salami *et al.*, 2016; Liu *et al.*, 2017), the artificial PVC wings (VT) proposed here offer a much larger plastic deformation range shown in Fig. 15; i.e. the wings do not crack immediately upon yielding. For instance, VT-1 does not undergo a fracture even at maximum wing displacement ($\Delta_{max} = 100$ mm) spanwise, implying a deformation rate of >97.6% that is almost double the rate (57.9%) obtained on an artificial *cicada* wing spanwise in Liu *et al.* (2017). VT-1c and VT-1gd, on the other hand, are much lighter with half the undesirable rigidity of VT-1; hence, they are more agile and flexible, recording a deformation rate of >148.2% and >135.8%, respectively, without damage. Although VT-1gd is slightly vulnerable near the wing root due to a major skin reduction seen in Fig. 15, the cellophane reinforcements compensate for this weakness and hence the prototype performs satisfactorily. It must be noted that due to high resilience of the cellophane reinforcements, fractures almost always occur on the wing frame towards the root. In particular, this property is highly favourable in the aerial applications where a trade-off strategy is necessary to maintain a balanced rigidity–flexibility ratio simultaneously preventing weight overloading and irreversible fatigue-induced fracture failures while airborne.

## 6 Discussion

As mentioned earlier, detailed influence and effects of various factors on mechanical properties of the prototypes are discussed in this section. Initially, a preliminary evaluation of aesthetics and consistency determines the selection of the appropriate prototypes for further analysis. Specifically, the significance of corrugations and the 15-micron wing membrane (cellophane reinforcement) is explored apart from the detailed comparative study of the wings designed by a nature-inspired supervised computer (VT-1gd), a nature-inspired engineer (VT-1c), and the nature itself (*locust* forewing). Since a wing is continuously subjected to torsional, compressive, and bending deformations while airborne, we determine the flexural stiffness and maximum deformation rate in both spanwise and chordwise direction to evaluate our prototypes' flexibility. The obtained results quantified in Table 3 are proven to be aeronautically favourable in terms of maintaining a more balanced trade-off strategy between the stiffness and flexibility of each prototype when compared to their counterparts presented in the related literature (Tanaka & Wood, 2010; Tanaka *et al.*, 2015; Salami *et al.*, 2016, 2020; Sivasankaran & Thomas, 2016; Liu *et al.*, 2017). This is speculated to be resulting from the main objective of the related research being focused on the biomimicry of natural wing aesthetics and mechanical properties, rather than focusing on the practicalities to develop aerodynamically functional wing prototypes.

**Table 3:** Mechanical properties of the fabricated artificial wing prototypes.

| Wing prototype | Wing mass (mg) | Profile thickness (μm) | Flexural stiffness ($Nm^2$) | |
|---|---|---|---|---|
| | | | Spanwise | Chordwise |
| locust | 12.4 | ~50 | $9.77 \times 10^{-9}$ | $5.96 \times 10^{-11}$ |
| VT-1 | 2019 | 150 | $1.27 \times 10^{-3}$ | $4.49 \times 10^{-4}$ |
| VT-2 | 2085 | 150 | $1.70 \times 10^{-3}$ | $4.82 \times 10^{-4}$ |
| VT-1p | 376 | 150 | $5.67 \times 10^{-5}$ | $2.96 \times 10^{-6}$ |
| VT-1c | 667 | 150 | $1.34 \times 10^{-4}$ | $5.67 \times 10^{-6}$ |
| VT-1cs | 586 | 150 | $1.07 \times 10^{-4}$ | $4.44 \times 10^{-6}$ |
| VT-1gd | 744 | 150 | $1.23 \times 10^{-4}$ | $3.29 \times 10^{-5}$ |
| VT-1gds | 482 | 150 | $9.20 \times 10^{-5}$ | $2.55 \times 10^{-5}$ |
| VT-2gd | 603 | 250 | $2.06 \times 10^{-4}$ | $3.12 \times 10^{-5}$ |
| VT-2gds | 341 | 250 | $1.74 \times 10^{-4}$ | $6.80 \times 10^{-5}$ |

It is evident from the graph in Fig. 14 that the flexural stiffness rises with an increase in wing size, thickness, and density. This correlation is demonstrated by the triangular and plus marker plots representing uncut full 250- and 300-μm-thick PVC wings (VT-2, -2gd, -2gds) on the top right of the graph. The laser cut 150-μm VT-1c,1gd prototypes, on the other hand, deliver an optimum balance of flexibility and rigidity since the artificial wings are sturdy enough to bear a 2.0 factor of safety with 89 and 67% slashed stiffness and mass, respectively. Additionally, due to the increased flexibility and reduced plastic membrane, the obtained maximum deformation rate for laser-cut wings (>148.2%) is improved by 50.6% and 90.3% compared to the uncut VT wings and an artificial *cicada* wing (Liu *et al.*, 2017), respectively. Although the computer-generated CAsD prototype (VT-1gd) is novel and innovative with even a slightly reduced (14%) stiffness and deformation rate (135.8%), its underlying technology is in nascent stages of development with an immense potential for future improvements. In an overall evaluation, the bioinspired engineer-designed prototype (VT-1c) outperforms other designs in this study by a small margin, and peer models from literature by a wider one. Therefore, this artificial wing sharing most similarity in attributes such as corrugations, planform, and thickness when compared to its counterpart in nature is best recommended for future experimental aerodynamic studies.

Downloaded from https://academic.oup.com/jcde/article/8/5/1191/6347742 by National Science & Technology Library Root Admin user on 27 August 2021

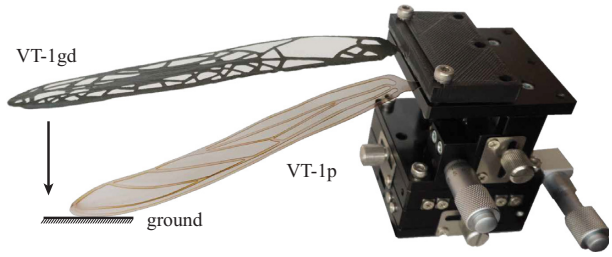


**Figure 16:** Illustration of an unformed 150-μm PVC sheet versus its thermoformed corrugated counterpart suspended from wing roots to highlight the significance of corrugations on wing integrity.

### 6.1 Effects of corrugations

In contrast to most of the bioinspired artificial wings developed in the literature (Perez-Rosado *et al.*, 2015; Sivasankaran & Thomas, 2016; Salami *et al.*, 2020), this research proposes a combination of fabrication techniques that cast natural wing corrugations precisely onto the proposed prototypes. Corrugations are found to be significant aerodynamically (Isakhani *et al.*, 2021b), which is inevitably correlated with the mechanical properties. To understand the role of these corrugations in maintaining the structural integrity of the wings, an unformed 150-μm PVC sheet is laser cut according to VT-1c contours to develop the VT-1p planar prototype whose *EI* is found to be closest to that of the real *locust* wing's stiffness when compared to the rest of the prototypes. However, as seen in Fig. 16, it is overly flexible, failing to withstand its own weight against gravity (not remaining erect), let alone withstanding the aerodynamic loads. This simplistic qualitative analysis missed in most of the related work emphasizes the significance and requirement of corrugations clearly appreciated by the vacuum thermoformed prototypes (VTs) to maintain a balanced ratio of flexibility–rigidity for real-world micro aerial robot applications.

### 6.2 Effects of wing membrane

Another vital feature of the proposed artificial wings in this study is the implementation of 15-micron PVC wrap used as wing membrane that significantly minimized weight by 67%, and improved flexibility by 90% for the VT-1 prototype when compared to its uncut and unwrapped counterpart (VT-1c). This 15-μm-thick wrap is commonly called cellophane sheet that is made of regenerated cellulose. Since it is extremely thin and transparent, the wrapped and unwrapped wing frames are not visually distinguishable in a pictorial illustration. However, the subtle and resilient nature of cellophane ensures great mouldability highly desirable for retaining accurate corrugations guided by the venations. As seen in Fig. 14, the wrapper reinforced (VT-1c, -1gd, -2gd) and unwrapped frame (VT-1cs, -1gds, -2gds) wings are represented by the filled and hollow markers, respectively. It is evident that the prototypes depicted by filled markers are 20–35% less flexible, and 10–30% heavier compared to their unwrapped counterparts. However, this increase in stiffness and weight is negligible when considering the integration of such an imperative part to achieve a functional wing prototype rather than a hollow exoskeletal structure. Hence, it can be concluded that the readily available and affordable combination of additive manufacturing, vacuum thermoforming, and a laser cutting machine could potentially be implemented in the mass production of the mechanically optimum (resilient, light) and disposable wings for the gliding/flapping micro aerial vehicle applications.

## 7 Conclusion

This study explores the application of the novel CAsD technology to generate bioinspired artificial wing design concepts with improved mechanical properties. Also, a conventional CAD-based model is developed to draw conclusions on the efficiency of each method. To facilitate a reliable process of performance evaluation, the design concepts are fabricated into distinct prototypes subjected to a standard experimental investigation of their mechanical properties. The computer-generated CAsD wing prototypes (VT-1gd,2gd) performed exceptionally well compared to the literature, with 78% increase in maximum deformation rate and 14% reduced stiffness compared to the CAD-based prototype (VT-1c). However, the bioinspired CAD wing (VT-1c) outperformed CAsD in the overall evaluation due to its solution consistency. The novel CAsD technology has plenty of potential to grow and this study proves that this is the future of CAD. Ultimately, a comparative study is provided to emphasize the influence and significance of each component of the proposed wing prototypes such as corrugations and few micron PVC membrane reinforcements. The extension of this research shall focus on a comprehensive PIV-based aerodynamic analysis of the recommended wing prototype.

## Acknowledgment

The authors would like to thank the anonymous reviewers for their valuable suggestions. This work is supported by EU Horizon 2020 projects STEP2DYNA (Grant No. 691154) and ULTRACEPT (Grant No. 778062).

## Author contribution

H.I., N.B., and S.Y. designed the study and performed the computational FEA, and drafted and critically revised the manuscript; H.I. and Q.B. performed the process of GD and produced meshed outcomes; H.I. and S.Y. conducted the process of natural wing scanning, digital reconstruction, fabrication, and post-processing; H.I., N.B., and Q.B. performed the experimental mechanical testing of the prototypes. All the authors gave final approval for publication.

## Conflict of interest statement

None declared.

## References

Autodesk, (2018). Generative design at Airbus.

Baker, H., (1744). *The microscope made easy*. University of Michigan Library.

Baker, P. S., & Cooter, R. J., (1979). The natural flight of the migratory locust, locusta migratoria L. II. Gliding. *Journal of Comparative Physiology*, *131*, 89–94.

Bao, X. Q., & Cattan, E., (2011). Golden ratio-based and tapered Diptera inspired wings: Their design and fabrication using standard MEMS technology. *Journal of Bionic Engineering*, *8*(2), 174–180.

Bao, X. Q., Bontemps, A., Grondel, S., & Cattan, E., (2011). Design and fabrication of insect-inspired composite wings for MAV

Downloaded from https://academic.oup.com/jcde/article/8/5/1191/6347742 by National Science & Technology Library Root Admin user on 27 August 2021

application using MEMS technology. *Journal of Micromechanics and Microengineering*, *21*(12), 1–16.

Broering, T. M., & Lian, Y. S., (2012). The effect of phase angle and wing spacing on tandem flapping wings. *Acta Mechanica Sinica*, *28*(6), 1557–1571.

Broering, T. M., Lian, Y., & Henshaw, W., (2012). Numerical investigation of energy extraction in a tandem flapping wing configuration. *AIAA Journal*, *50*(11), 2295–2307.

Ceruti, A., Marzocca, P., Liverani, A., & Bil, C., (2019). Maintenance in aeronautics in an industry 4.0 context: The role of augmented reality and additive manufacturing. *Journal of Computational Design and Engineering*, *6*(4), 516–526.

Chakrabarti, A., Shea, K., Stone, R., Cagan, J., Campbell, M., Hernandez, N. V., & Wood, K. L., (2011). Computer-based design synthesis research: An overview. *Journal of Computing and Information Science in Engineering*, *11*(2), 021003–021008.

Chen, Y. H., & Skote, M., (2016). Gliding performance of 3-D corrugated dragonfly wing with spanwise variation. *Journal of Fluids and Structures*, *62*, 1–13.

Combes, S. A., & Daniel, T. L., (2003). Flexural stiffness in insect wings I. Scaling and the influence of wing venation. *Journal of Experimental Biology*, *206*(17), 2979–2987.

D'Amato, E., Daniele, E., Mallozzi, L., & Petrone, G., (2012a). Equilibrium strategies via GA to Stackelberg Games under multiple follower's best reply. *International Journal of Intelligent Systems*, *27*, 74–85.

D'Amato, E., Daniele, E., Mallozzi, L., Petrone, G., & Tancredi, S., (2012b). A hierarchical multimodal hybrid Stackelberg-Nash GA for a leader with multiple followers game. In *Dynamics of information systems: Mathematical foundations*(Vol. *20*, pp. 267–280). Springer.

Della Vecchia, P., Daniele, E., & D'Amato, E., (2014). An airfoil shape optimization technique coupling PARSEC parameterization and evolutionary algorithm. *Journal of Aerospace Sciences and Technologies*, *32*(1), 103–110.

Du, G., & Sun, M., (2012). Aerodynamic effects of corrugation and deformation in flapping wings of hovering hoverflies. *Journal of Theoretical Biology*, *300*, 19–28.

Ellington, C. P., (1984a). The aerodynamics of hovering insect flight. III. Kinematics. *Philosophical Transactions of the Royal Society of London. Series B, Biological Sciences*, *305*(1122), 41–78.

Ellington, C. P., (1984b). The aerodynamics of hovering insect flight. IV. Aerodynamic mechanisms. *Philosophical Transactions of the Royal Society of London. Series B, Biological Sciences*, *305*(1122), 79–113.

Ellington, C. P., (1984c). The aerodynamics of hovering insect flight. VI. Lift and power requirements. *Philosophical Transactions of the Royal Society of London. Series B, Biological Sciences*, *305*(1122), 145–181.

Engelmann, S., (2012). Basics of thermoforming and thermoplastics. In R. Grossman, D. Nwabunma, & S. Engelmann (Eds.), *Advanced thermoforming*(pp. 5–11). Wiley.

Haefer, J., & Rudolph, S., (2005). Satellite design by design grammars. *Aerospace Science and Technology*, *9*(1), 81–91.

Haupt, R. L., & Haupt, S. E., (1998). *Practical genetic algorithms*. Wiley-Interscience.

Helms, B., & Shea, K., (2012). Computational synthesis of product architectures based on object-oriented graph grammars. *Journal of Mechanical Design*, *134*(2), 021008–021022.

Henningsson, P., Hedenström, A., & Bomphrey, R. J., (2014). Efficiency of lift production in flapping and gliding flight of swifts. *PLoS ONE*, *9*(2), 1–7.

Henningsson, P., Michaelis, D., Nakata, T., Schanz, D., Geisler, R., Schröder, A., & Bomphrey, R. J., (2015). The complex aerodynamic footprint of desert locusts revealed by large-volume tomographic particle image velocimetry. *Journal of the Royal Society Interface*, *12*(108), 1–11.

Hoisl, F., & Shea, K., (2011). An interactive, visual approach to developing and applying parametric three-dimensional spatial grammars. *AI EDAM*, *25*(4), 333–356.

Hou, D., Yin, Y., Zhong, Z., & Zhao, H., (2015). A new torsion control mechanism induced by blood circulation in dragonfly wings. *Bioinspiration and Biomimetics*, *10*(1), 1–10.

Isakhani, H., Xiong, C., Yue, S., & Chen, W., (2020a). A bioinspired airfoil optimization technique using Nash genetic algorithm. In *Proceedings of the 17th International Conference on Ubiquitous Robots (UR)*(pp. 506–513).

Isakhani, H., Yue, S., Xiong, C., Chen, W., Sun, X., & Liu, T., (2020b). Fabrication and mechanical analysis of bioinspired gliding-optimized wing prototypes for micro aerial vehicles. In *Proceedings of the 5th International Conference on Advanced Robotics and Mechatronics (ICARM)*(pp. 602–608).

Isakhani, H., Xiong, C., Chen, W., & Yue, S., (2021a). Towards locust-inspired gliding wing prototypes for micro aerial vehicle applications. *Journal of Royal Society Open Science*, *1*(accepted), 1–16.

Isakhani, H., Yue, S., Xiong, C., & Chen, W., (2021b). Aerodynamic analysis and optimization of gliding locust wing using Nash genetic algorithm. *AIAA Journal*, *1*(accepted), 1–25.

Jansson, D. G., & Smith, S. M., (1991). Design fixation. *Design Studies*, *12*(1), 3–11.

Jin, T., Goo, N. S., & Park, H. C., (2010). Finite element modeling of a beetle wing. *Journal of Bionic Engineering*, *7*, 145–149.

Kesel, A. B., (2000). Aerodynamic characteristics of dragonfly wing sections compared with technical aerofoils. *Journal of Experimental Biology*, *203*, 3125–3135.

Kim, J., & Yoo, D. J., (2020). 3D printed compact heat exchangers with mathematically defined core structures. *Journal of Computational Design and Engineering*, *7*(4), 527–550.

Kim, J. K., & Han, J. H., (2014). A multibody approach for 6-DOF flight dynamics and stability analysis of the hawkmoth Manduca sexta. *Bioinspiration and Biomimetics*, *9*(1), 1–22.

Kim, W. K., Ko, J. H., Park, H. C., & Byun, D., (2009). Effects of corrugation of the dragonfly wing on gliding performance. *Journal of Theoretical Biology*, *260*(4), 523–530.

Koehler, C., Liang, Z., Gaston, Z., Wan, H., & Dong, H., (2012). 3D reconstruction and analysis of wing deformation in free-flying dragonflies. *Journal of Experimental Biology*, *215*(17), 3018–3027.

Levy, D. E., & Seifert, A., (2009). Simplified dragonfly airfoil aerodynamics at Reynolds numbers below 8000. *Journal of Physics of Fluids*, *21*(7), 071901.

Lin, Y.-S., Shea, K., Johnson, A., Coultate, J., & Pears, J., (2009). A method and software tool for automated gearbox synthesis. In *Proceedings of the ASME International Design Engineering Technical Conferences (IDETC/CIE'09)*(pp. 111–121).

Lin, E., Li, Y., Ortiz, C., & Boyce, M. C., (2014). 3D printed, bio-inspired prototypes and analytical models for structured suture interfaces with geometrically-tuned deformation and failure behavior. *Journal of the Mechanics and Physics of Solids*, *73*, 166–182.

Liu, Z., Yan, X., Qi, M., Zhu, Y., Huang, D., Zhang, X., & Lin, L., (2017). Artificial insect wings with biomimetic wing morphology and mechanical properties. *Bioinspiration and Biomimetics*, *12*(5), 1–13.

Lorenz, M. W., (2009). Migration and trans-Atlantic flight of locusts. *Journal of Quaternary International*, *196*(2), 4–12.

Downloaded from https://academic.oup.com/jcde/article/8/5/1191/6347742 by National Science & Technology Library Root Admin user on 27 August 2021

Luca, M., Mintchev, S., Heitz, G., Noca, F., & Floreano, D., (2017). Bioinspired morphing wings for extended flight envelope and roll control of small drones. *Interface Focus*, *7*, 1–11.

Luo, G., & Sun, M., (2005). Effects of corrugation and wing planform on the aerodynamic force production of sweeping model insect wings. *Acta Mechanica Sinica*, *21*(6), 531–541.

Macdonald, S., (2006). Thermoforming. In C. A. Harper (Ed.), *Handbook of plastic processes*(pp. 291–304). John Wiley & Sons.

Meng, X., & Sun, M., (2011). Aerodynamic effects of corrugation in flapping insect wings in forward flight. *Journal of Bionic Engineering*, *8*(2), 140–150.

Nash, J., (1951). Non-cooperative games. *Annals of Mathematics*, *54*(2), 286–295.

Nguyen, Q. V., Ha, N. S., Park, H. C., & Goo, N. S., (2011). Composite artificial wing mimicking a beetle hind-wing. In *Proceeding of the International Conference on Composite Materials*(pp. 1–6).

Nguyen, C. H. P., Kim, Y., Do, Q. T., & Choi, Y., (2021). Implicit-based computer-aided design for additively manufactured functionally graded cellular structures. *Journal of Computational Design and Engineering*, *8*, 813–823.

Nourbakhsh, M., Morris, N., Bergin, M., Lorio, F., & Grandi, D., (2016). Embedded sensors and feedback loops for iterative improvement in design synthesis for additive manufacturing. In *Proceedings of the ASME International Design Engineering Technical Conferences and Computers and Information in Engineering*(pp. 1–9).

Park, J. H., Yoon, K. J., & Park, H. C., (2007). Development of biomimetic composite wing structures and experimental study on flapping characteristics. In *IEEE International Conference on Robotics and Biomimetics (ROBIO)*(pp. 25–30).

Pass, G., (2018). Beyond aerodynamics: The critical roles of the circulatory and tracheal systems in maintaining insect wing functionality. *Arthropod Structure & Development*, *47*(4), 391–407.

Perez-Rosado, A., Gehlhar, R. D., Nolen, S., Gupta, S. K., & Bruck, H. A., (2015). Design, fabrication, and characterization of multifunctional wings to harvest solar energy in flapping wing air vehicles. *Smart Materials and Structures*, *24*(6), 1–15.

Pornsin-sirirak, T. N., Tai, Y. C., Nassef, H., & Ho, C. M., (2001). Titanium-alloy MEMS wing technology for a micro aerial vehicle application. *Sensors and Actuators A*, *89*(2), 95–103.

Rajabi, H., Shafiei, A., Darvizeh, A., & Gorb, S. N., (2016). Resilin microjoints: A smart design strategy to avoid failure in dragonfly wings. *Scientific Reports*, *6*, 1–5.

Rayleigh, J. W. S., (1883). The soaring of birds. *Nature*, *27*, 534–535.

Richter, C., & Lipson, H., (2011). Untethered hovering flapping flight of a 3D-printed mechanical insect. *Artificial Life*, *17*(2), 73–86.

Rival, D. E., Hass, G., & Tropea, C., (2011). Recovery of energy from leading- and trailing-edge vortices in tandem-airfoil configurations. *Journal of Aircraft*, *48*(1–2), 203–211.

Rubaiat, H. K., Grossman, T., Cheong, H., Hashemi, A., & Fitzmaurice, G., (2017). DreamSketch: Early stage 3D design explorations with sketching and generative design. In *Proceedings of the 30th Annual ACM Symposium*(pp. 1–14).

Salami, E., Ganesan, P. B., Ward, T. A., Viyapuri, R., & Romli, F. I., (2016). Design and mechanical analysis of a 3D-printed biodegradable biomimetic micro air vehicle wing. *IOP Conf. Series: Materials Science and Engineering*, *152*, 1–8.

Salami, E., Ward, T. A., Montazer, E., & Nik Ghazali, N. N., (2020). Nanoindentation analysis comparing dragonfly-inspired biomimetic micro-aerial vehicle (BMAV) wings. *International Journal of Bio-Inspired Computation*, *16*(2), 111–120.

Shang, J. K., Combes, S. A., Finio, B. M., & Wood, R. J., (2009). Artificial insect wings of diverse morphology for flapping-wing micro air vehicles. *Bioinspiration and Biomimetics*, *4*(3), 1–6.

Sharma, G. K., & Gurumoorthy, B., (2020). Iso-material contour representation for process planning of heterogeneous object model. *Journal of Computational Design and Engineering*, *7*(4), 498–513.

Shea, K., Aish, R., & Gourtovaia, M., (2005). Towards integrated performance-driven generative design tools. *Automation in Construction*, *14*(2), 253–264.

Sivasankaran, P. N., & Thomas, A. W., (2016). Spatial network analysis to construct simplified wing structural models for Biomimetic Micro Air Vehicles. *Aerospace Science and Technology*, *49*, 259–268.

Sobieczky, H., (1998). Parametric airfoils and wings. In *Notes on numerical fluid mechanics*(Vol. *68*, pp. 71–88). Springer.

Takeda, H., Ohtake, Y., & Suzuki, H., (2020). 3D printing CFD simulation results using structural mechanics. *Journal of Computational Design and Engineering*, *7*(3), 287–293.

Tanaka, H., & Wood, R. J., (2010). Fabrication of corrugated artificial insect wings using laser micromachined molds. *Journal of Micromechanics and Microengineering*, *20*(7), 1–8.

Tanaka, H., Matsumoto, K., & Shimoyama, I., (2007). Fabrication of a three-dimensional insect-wing model by micromolding of thermosetting resin with a thin elastmeric mold. *Journal of Micromechanics and Microengineering*, *17*(12), 2485–2490.

Tanaka, H., Okada, H., Shimasue, Y., & Liu, H., (2015). Flexible flapping wings with self-organized microwrinkles. *Bioinspiration and Biomimetics*, *10*(4), 1–13.

Taylor, G. K., & Thomas, A. L. R., (2003). Dynamic flight stability in the desert locust Schistocerca gregaria. *Journal of Experimental Biology*, *206*, 2803–2829.

Tsai, C.-C., Childers, R. A., Shi, N. N., Ren, C., Pelaez, J. N., Bernard, G. D., Pierce, N. E., & Yu, N., (2020). Physical and behavioral adaptations to prevent overheating of the living wings of butterflies. *Nature Communications*, *11*, 1–14.

Walker, G., (1925). The flapping flight of birds. *Journal of Royal Aeronautical Society*, *29*(179), 590–594.

Walker, S. M., Thomas, A. L. R., & Taylor, G. K., (2009). Deformable wing kinematics in the desert locust: How and why do camber, twist and topography vary through the stroke? *Journal of the Royal Society Interface*, *6*(38), 735–747.

Xiang, J., Du, J., Li, D., & Liu, K., (2016). Aerodynamic performance of the locust wing in gliding mode at low Reynolds number. *Journal of Bionic Engineering*, *13*(2), 249–260.

Yang, Y., Ohtake, Y., & Suzuki, H., (2021). Mesh processing for improved perceptual quality of 3D printed relief. *Journal of Computational Design and Engineering*, *8*(1), 115–124.

Youmans, R. J., & Arciszewski, T., (2014). Design fixation: A cloak of many colors. In *Design computing and cognition '12*(pp. 115–129). Springer.

Zhang, Y., & Moon, S. K., (2021). Data-driven design strategy in fused filament fabrication: Status and opportunities. *Journal of Computational Design and Engineering*, *8*, 489–509.

Downloaded from https://academic.oup.com/jcde/article/8/5/1191/6347742 by National Science & Technology Library Root Admin user on 27 August 2021